

Altermagnetism-driven type-III multiferroicity in $CrSiTe_3$-based van der Waals structures

Si-Yuan Zhang(张思远), Cai-Xin Zhang(张才鑫), Liang-Po Tang(唐梁坡), Qian-Ze Li(黎前泽), Ke-Qiu Chen(陈克求), Li-Ming Tang(唐黎明)

Citation: Chin. Phys. B. 35, 097501 (2026). DOI: 10.1088/1674-1056/ae74bb |
CSTR: 32038.14.CPB.ae74bb
http://cpb.iphy.ac.cn; http://iopscience.iop.org/cpb

What follows is a list of articles you may be interested in

G-type antiferromagnetic structure in the metallic d-wave altermagnet Rb1−δV2Te2O

Wu Xie(谢武), Changchao Liu(刘长超), Fayuan Zhang(张发远), Zhenhong Tan(谭振宏), Wenhai Ji(季文海), Nan Zhao(赵南), Lingxiang Bao(鲍伶香), Dong Zhang(张栋), Feiran Shen(沈斐然), Hao Wang(王浩), Rong Du(杜蓉), Lunhua He(何伦华), Guanghan Cao(曹光旱), Chaoyu Chen(陈朝宇), Ping Miao(缪平)
Chin. Phys. B. 35, 087503 (2026). DOI: 10.1088/1674-1056/ae8f1a | CSTR: 32038.14.CPB.ae8f1a

Higher-order topological semimetal induced by altermagnet

Dengfeng Wang(王登风), Xiang Ji(吉祥), Sen Cui(崔森)
Chin. Phys. B. 35, 077510 (2026). DOI: 10.1088/1674-1056/ae6b35 | CSTR: 32038.14.CPB.ae6b35

Design of magnetoelectric coupling in ferroelectric metal

Wang Zhang(张旺), Xue-Zeng Lu(逯学曾)
Chin. Phys. B. 35, 077506 (2026). DOI: 10.1088/1674-1056/ae6173 | CSTR: 32038.14.CPB.ae6173

Recent progress on electron- and magnon-mediated torques

Jia-Min Lai(来嘉敏), Bingyue Bian(边冰玥), Zhonghai Yu(于忠海), Kaiwei Guo(郭凯卫), Yajing Zhang(张雅静), Pengnan Zhao(赵鹏楠), Xiaoqian Zhang(张霄倩), Chunyang Tang(汤春阳), Jiasen Cao(曹家森), Zhiyong Quan(全志勇), Fei Wang(王飞), Xiaohong Xu(许小红)
Chin. Phys. B. 34, 107501 (2025). DOI: 10.1088/1674-1056/add909 | CSTR: 32038.14.CPB.add909

Alternating spin splitting of electronic and magnon bands in two-dimensional altermagnetic materials

Qian Wang(王乾), Da-Wei Wu(邬大为), Guang-Hua Guo(郭光华), Meng-Qiu Long(龙孟秋), Yun-Peng Wang(王云鹏)
Chin. Phys. B. 33, 097507 (2024). DOI: 10.1088/1674-1056/ad6425

RAPID COMMUNICATION

Altermagnetism-driven type-III multiferroicity in $CrSiTe_3$-based van der Waals structures

Si-Yuan Zhang(张思远)[1,†], Cai-Xin Zhang(张才鑫)[2,†], Liang-Po Tang(唐梁坡)[3], Qian-Ze Li(黎前泽)[4], Ke-Qiu Chen(陈克求)[1], and Li-Ming Tang(唐黎明)[1,‡]

[1] *Department of Applied Physics, School of Physics and Electronics, Hunan University, Changsha* 410082, *China*
[2] *School of Science, Hunan Institute of Technology, Hengyang* 421002, *China*
[3] *Guangdong University of Education, Guangzhou* 510303, *China*
[4] *Department of Physics and Chemistry, Hunan First Normal University, Changsha* 410205, *China*

(Received 18 May 2026; revised manuscript received 25 May 2026; accepted manuscript online 29 May 2026)

Altermagnets exhibit unique nonrelativistic spin splitting and zero net magnetization, but achieving active electrical control over their magnetic states remains a primary challenge for spintronic applications. In this work, using first-principles calculations, we demonstrate that interlayer sliding in $CrSiTe_3$-based van der Waals structures provides an effective route to engineer type-III multiferroicity driven by the intrinsic coupling of altermagnetism with sliding ferroelectricity. In a $CrSiTe_3/SnS_2$ heterostructure, breaking the inversion symmetry that connects the magnetic sublattices drives a transition from a conventional antiferromagnetic state to an altermagnetic state, accompanied by the emergence of out-of-plane polarization and nonrelativistic spin splitting. However, the absence of an inversion symmetry restoration pathway prevents reversible control of both polarization and spin orientation. To overcome this limitation, we design a $SnS_2/CrSiTe_3/SnS_2$ sandwich structure, where interlayer sliding enables switching between inversion-symmetric and inversion-broken states. This process simultaneously reverses electric polarization and spin orientation, realizing spin-polarization locking in an altermagnetic system. Furthermore, type-III multiferroicity is achieved in bilayer $CrSiTe_3$ without external substrates. These results establish a general strategy for integrating altermagnetism with sliding ferroelectricity and provide a viable route toward electrically controllable altermagnetic spintronic applications.

Keywords: altermagnetism, sliding ferroelectricity, antiferromagnetism, type-III multiferroics

PACS: 75.50.Ee, 75.85.+t, 77.80.–e

DOI: 10.1088/1674-1056/ae74bb **CSTR:** 32038.14.CPB.ae74bb

1. Introduction

Altermagnets (AM), revealed as the third class of collinear magnets following ferromagnets and antiferromagnets (AFM), have emerged as a frontier in contemporary condensed matter physics and spintronics.[1–4] Unlike those in conventional AFMs, the antiparallel spin sublattices in AM are connected via rotational or mirror symmetry operations ($\mathcal{M}$), rather than by translational or inversion symmetry ($\mathcal{P}$) operations.[5–7] This unique crystallographic symmetry protection endows AMs with the dual characteristics of a zero net macroscopic magnetization and an alternating distribution of nonrelativistic spin polarization in momentum space. Consequently, AM combines the advantages of ferromagnets (e.g., spin-polarized bands, readable signals) and AFM (e.g., high intrinsic frequencies, weak response to external fields), making them ideal candidates for ultrafast, high-density information storage.[8–10] Nevertheless, achieving rational design and active control of the AM state, particularly electric-field-controlled spin modulation, remains a major challenge for practical applications.

To realize electrical control of altermagnetic (AM) states, multiferroic systems have attracted extensive attention due to their ability to establish coupling between electric polarization and magnetic order. However, conventional type-I multiferroics usually exhibit weak magnetoelectric coupling, whereas type-II multiferroics, despite possessing stronger coupling, are often accompanied by relatively small polarization and low Curie temperatures.[11–15] To overcome these limitations, the concept of "type-III multiferroicity" has recently been proposed, aiming to establish deterministic coupling among symmetry, electronic, spin, and lattice degrees of freedom through intrinsic correlations. At present, three representative frameworks have been developed to describe the physical nature of type-III multiferroicity. The first is the "causal-driven" framework, exemplified by Jiang *et al.* in Cu-InI_3, where ferroelectric distortions induce magnetism through modulation of orbital overlap.[16] The second is the "homologous-entanglement" framework, as demonstrated by Wang *et al.* in $TiCdO_4$, where ferroelectric and magnetic orders originate simultaneously from competing electronic occupations.[17] The

[†] These authors contributed equally to this work.
[‡] Corresponding author. E-mail: lmtang@semi.ac.cn
© 2026 Chinese Physical Society and IOP Publishing Ltd. All rights, including for text and data mining, AI training, and similar technologies, are reserved.

third is the "symmetry-locking" framework, whose essential feature lies not in a causal or common-origin relationship between ferroelectricity and magnetism, but in a one-to-one correspondence enforced by crystal symmetry.[18] Within the symmetry-locking framework, ferroelectric switching is mathematically equivalent to an effective time-reversal operation acting on the electronic band structure, thereby enabling synchronous reversal of spin polarization and electric polarization. For example, Sun *et al.* demonstrated in bilayer $MnPSe_3$ that interlayer-sliding-induced polarization reversal is accompanied by a 180° reversal of altermagnetic spin polarization, establishing a deterministic "spin–polarization locking" relationship.[18] Since the nonrelativistic spin splitting in AM strongly depends on crystal and magnetic symmetries, such a symmetry-locking mechanism provides an ideal platform for achieving reversible electrical control of AM states.

Since the spin degeneracy in many AFM systems is protected by inversion-related symmetries, an applied electric field, owing to its intrinsic polarity, can reduce the crystal symmetry and break spatial inversion symmetry. This symmetry reduction can lift the protected spin degeneracy and thereby enable transitions from conventional AFM states to AM states when the remaining symmetries satisfy the altermagnetic condition.[7,19–21] Sliding ferroelectricity, arising from relative interlayer displacements in van der Waals (vdW) structures, provides an intrinsic mechanism to generate out-of-plane polarization and modulate $\mathcal{P}$ symmetry without significantly altering the electronic structure of individual layers.[22–26] The coupling of AM, which hosts symmetry-protected spin splitting, and sliding ferroelectricity, which enables dynamic control of $\mathcal{P}$ symmetry, fundamentally constitutes a novel platform for type-III multiferroicity.

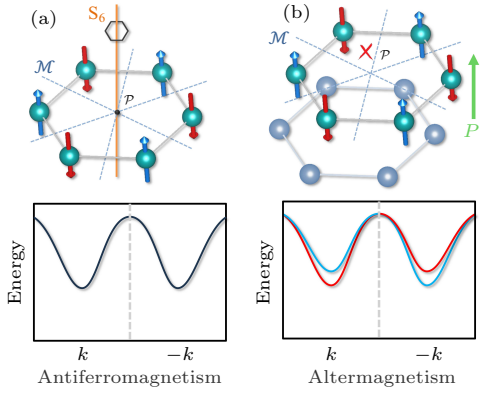


Fig. 1. Schematic illustrations of the Néel-type magnetic order and corresponding band structures for monolayer $CrSiTe_3$ (a) and its vdW heterostructure (b). Monolayer $CrSiTe_3$ exhibits D_{3d} symmetry, where the antiparallel magnetic sublattices are related by mirror symmetry ($\mathcal{M}$), rotoinversion symmetry (S_6), and inversion symmetry ($\mathcal{P}$). Protected by the combined $\mathcal{PT}$ symmetry, the system exhibits a spin-degenerate antiferromagnetic state. Upon introducing an asymmetric substrate, the inversion symmetry $\mathcal{P}$ connecting the antiparallel magnetic sublattices is broken, thereby lifting the $\mathcal{PT}$-protected spin degeneracy and driving the transition from a conventional antiferromagnetic state to an altermagnetic state with momentum-dependent spin splitting.

Recent studies have demonstrated this concept in systems such as bilayer $MnPSe_3$[18] and sandwich heterostructures including $SnS_2/MnPSe_3/SnS_2$[27] and GaSe/$VPSe_3$/GaSe.[28] However, these systems generally exhibit relatively small spin-splitting energies, and the general applicability of such symmetry-driven mechanisms across different material platforms remains to be established.

Monolayer $CrSiTe_3$ exhibits exceptional structural stability and highly tunable electronic and magnetic properties,[29–32] serving as an ideal platform for symmetry-engineered spintronic functionalities. Monolayer $CrSiTe_3$ belongs to the D_{3d} point group, which preserves both $\mathcal{P}$ and time-reversal ($\mathcal{T}$) symmetries. This symmetry results in spin-degenerate states in the AFM configuration, as detailed in Fig. 1(a). Breaking $\mathcal{P}$ symmetry is crucial for realizing type-III multiferroicity in $CrSiTe_3$-based systems, while the $[\mathcal{C}_2||\mathcal{M}]$ symmetry connecting antiparallel spin sublattices stabilizes the altermagnetic (AM) state.

Consequently, SnS_2, which exhibits room-temperature sliding ferroelectricity (space group $P\bar{3}m1$, point group D_{3d}),[25] is introduced as a substrate for the construction of a vdW heterostructure. As a nonmagnetic semiconductor, the low-energy region of the electronic structure in SnS_2 primarily originates from Sn-5s and S-3p orbitals. Therefore, additional magnetic ordering is not introduced upon heterostructure formation, ensuring the stability of the AFM configuration within the $CrSiTe_3$ layer. The inequivalence of atomic environments at the heterointerface breaks the inversion symmetry $\mathcal{P}$ connecting the antiparallel magnetic sublattices, which lifts spin degeneracy and drives the transition to an AM state, while $\mathcal{M}$ symmetry between the antiparallel spin sublattices remains intact (Fig. 1(b)).

In this work, first-principles calculations are employed to systematically investigate the realization of type-III multiferroicity in vdW structures based on the two-dimensional AFM semiconductor $CrSiTe_3$. Our results show that, although the $CrSiTe_3/SnS_2$ heterostructure can successfully induce an AM transition, neither the polarization nor the spin orientation can be reversed. To overcome this limitation, we further construct a $SnS_2/CrSiTe_3/SnS_2$ sandwich structure, in which interlayer sliding enables the coupled manipulation of polarization magnitude and spin orientation, thereby realizing a type-III multiferroic state. Furthermore, we demonstrate the feasibility of achieving type-III multiferroicity in bilayer $CrSiTe_3$.

2. Results and discussion

We begin our investigation with the $CrSiTe_3/SnS_2$ bilayer heterostructures. According to the symmetry analysis described above, monolayer $CrSiTe_3$ is protected by the combined $\mathcal{PT}$ symmetry, exhibiting a strictly spin-degenerate AFM state. Although the zigzag-AFM state is slightly lower in

energy under the present computational conditions, the Néel-AFM configuration remains energetically competitive and can be stabilized through strain, interlayer coupling, or interface engineering.[30–32] Accordingly, we introduce SnS_2, which possesses room-temperature sliding ferroelectricity,[25] as a substrate to construct the $\sqrt{3}\times\sqrt{3}$ $SnS_2/1\times1$ $CrSiTe_3$ vdW heterostructure. Due to the small lattice mismatch of only 3.6%, the system effectively breaks $\mathcal{P}$ symmetry through interfacial interactions while maintaining structural stability.

Two representative high-symmetry stacking configurations, namely AB and BA stackings, are considered (Fig. 2). In the AB stacking, the Si–Si bonds within the $CrSiTe_3$ layer align along the out-of-plane (z) direction with the proximal S (or Te) atoms in the adjacent layer. In contrast, for the BA stacking, this collinear alignment occurs with the distal S (or Te) atoms of the neighboring layer. By applying an in-plane sliding to the bottom layer of AB stacking along the lattice vector direction ($\boldsymbol{r} = 1/3\boldsymbol{a}$), the interfacial atomic registry is modified, thereby transforming the system into the BA stacking configuration. At the heterointerface, the inequivalence of atomic environments at the interface breaks $\mathcal{P}$ symmetry, reducing the point-group symmetry from D_{3d} (of monolayer $CrSiTe_3$) to C_{3v}. This symmetry reduction provides the necessary condition for the emergence of an AM state within the $CrSiTe_3$-based system.

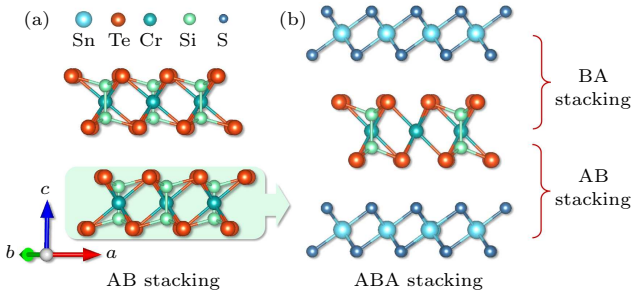


Fig. 2. Schematic illustrations of $CrSiTe_3$-based vdW structures. (a) AB-stacked $CrSiTe_3/CrSiTe_3$ bilayer homostructure. (b) ABA-stacking $SnS_2/CrSiTe_3/SnS_2$ sandwich heterostructure, in which the upper interface corresponds to BA stacking, while the lower interface corresponds to AB stacking.

Band structure calculations confirm that the BA-stacking $CrSiTe_3/SnS_2$ vdW heterostructure exhibits pronounced spin splitting along the K–K' path, even in the absence of spin-orbit coupling (see Fig. 3(a)). The corresponding high-symmetry points (Fig. S1) and computational details of the first-principles calculations are provided in Section 1 of the supplemental material[33] (see also Refs. [31,34–39] therein). Notably, modification of the interfacial atomic registry via interlayer sliding ($\boldsymbol{r} = 1/3\boldsymbol{a}$) allows for a significant enhancement of the spin-splitting energy near the Fermi level, increasing from approximately 0.5 meV in the BA stacking to 14 meV in the AB stacking (Fig. 3(c)).

To elucidate the physical origin of this variation, we analyze the charge density difference, defined as $\Delta\rho = \rho_{CrSiTe_3/SnS_2} - \rho_{CrSiTe_3} - \rho_{SnS_2}$. The results indicate that interfacial charge transfer occurs upon heterostructure formation, accompanied by a pronounced redistribution of charge density at the interface. This process leads to charge depletion around the less electronegative Te atoms and accumulation near the more electronegative S atoms, as illustrated in Figs. 3(b) and 3(d). This interlayer charge redistribution generates a net out-of-plane polarization pointing from the SnS_2 layer toward the $CrSiTe_3$ layer. Moreover, the charge density difference indicates more pronounced spatial charge redistribution (interfacial polarization) in the AB stacking, as evidenced by stronger and more extended charge accumulation at the interface. Furthermore, upon applying a vertical electric field of $E_z = 0.20$ V/Å, the spin-splitting energy changes only slightly (~ 2 meV), indicating that it is weakly affected by external perturbations.

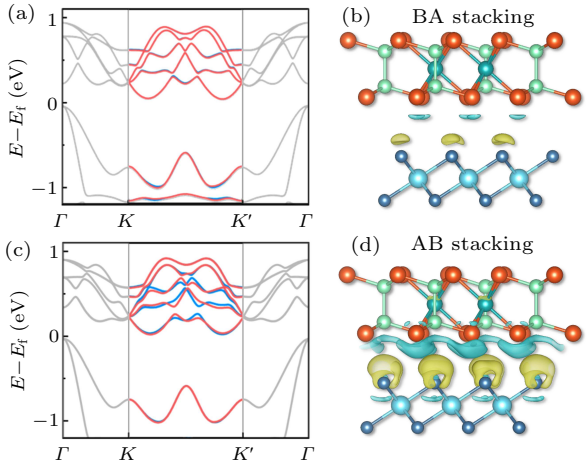


Fig. 3. Electronic band structures and charge density differences of the $CrSiTe_3/SnS_2$ heterostructure. (a) and (c) Spin-polarized band structures for the BA and AB stacking configurations, respectively, where blue (red) curves represent spin-up (spin-down) states. (b) and (d) Corresponding charge density difference distributions, in which yellow and blue regions denote charge accumulation and depletion, respectively. The isosurface value for the charge density difference is set to 4×10^{-4} e/Å^3.

Although the $CrSiTe_3/SnS_2$ heterojunction successfully hosts coexisting electric polarization and spin splitting, the absence of an inversion center in the bilayer heterojunction means that the directions of electric polarization and spin polarization cannot be fully reversed or switched off through simple interlayer sliding. This limitation implies that bilayer heterostructures alone are insufficient to achieve a fully switchable type-III multiferroic state with complete electrical control.

To overcome this limitation, a $SnS_2/CrSiTe_3/SnS_2$ sandwich structure is constructed by introducing symmetric SnS_2 layers on both sides of the $CrSiTe_3$ monolayer. In this system, $\mathcal{P}$ symmetry is determined by the relative interlayer stacking configuration, providing a tunable symmetry basis for magnetoelectric coupling. Considering that the interfacial electric dipoles at the $CrSiTe_3/SnS_2$ interfaces consistently point from SnS_2 toward $CrSiTe_3$, together with the atomic registry at the

interfaces, four representative high-symmetry configurations (ABA, ABA′, B_1, and B_2) are identified. In the ABA configuration, the upper and lower interfaces correspond to BA and AB stackings (Fig. 2(b)), respectively, whereas the ABA′ configuration exhibits the opposite arrangement, as illustrated in Fig. 4(a). Simultaneous sliding of both the top and bottom SnS_2 layers by $\boldsymbol{r} = -1/3\boldsymbol{a}$ transforms the system from ABA into the ABA′ stacking configuration. In the B_1 configuration, both interfaces adopt BA stacking, while in the B_2 configuration, both interfaces correspond to AB stacking.

The polarization mechanism in this sandwich structure is consistent with that of the bilayer system and originates from interfacial charge redistribution. However, due to the coupling between the top and bottom interfaces, the polarization exhibits a characteristic behavior of either constructive addition or mutual cancellation. Specifically, the ABA and ABA′ configurations exhibit net out-of-plane polarization along the $+z$ and $-z$ directions, respectively. In contrast, in the B_1 and B_2 configurations, interfacial dipoles cancel each other, resulting in zero net polarization.

Figure 4(a) shows two nonequivalent sliding pathways connecting the ABA and ABA′ configurations: path 1 (ABA→B_1→ABA′) and path 2 (ABA→B_2→ABA′), corresponding to sequential sliding of the bottom and top layers, and vice versa. The corresponding energy profiles (Fig. 4(b)) along the two sliding pathways reveal distinct intermediate states (B_1 and B_2) with different energetic characteristics. Along path 1, B_1 is a local minimum with an energy higher than those of the two stable states, ABA and ABA′, whereas along path 2, B_2 corresponds to the global minimum of the entire sliding process. The corresponding switching barriers, defined as the highest energy barriers that must be overcome during ferroelectric switching, are 69 meV and 66 meV for paths 1 and 2, respectively. These values are higher than those reported for the type-III multiferroic $SnS_2/MnPSe_3/SnS_2$ system,[27] suggesting enhanced stability of the ferroelectric states. Nevertheless, the barriers remain within the tens-of-meV range, implying that ferroelectric switching via interlayer sliding is still experimentally accessible under external electric fields.

Further symmetry analysis reveals that the ABA and ABA′ configurations break $\mathcal{P}$ symmetry due to the asymmetry between the top and bottom interfaces, reducing the point-group symmetry from D_{3d} to C_{3v}. In this non-centrosymmetric environment, the antiparallel spin sublattices are related only by $[\mathcal{C}_2||\mathcal{M}]$ symmetry, satisfying the symmetry requirements for AM.

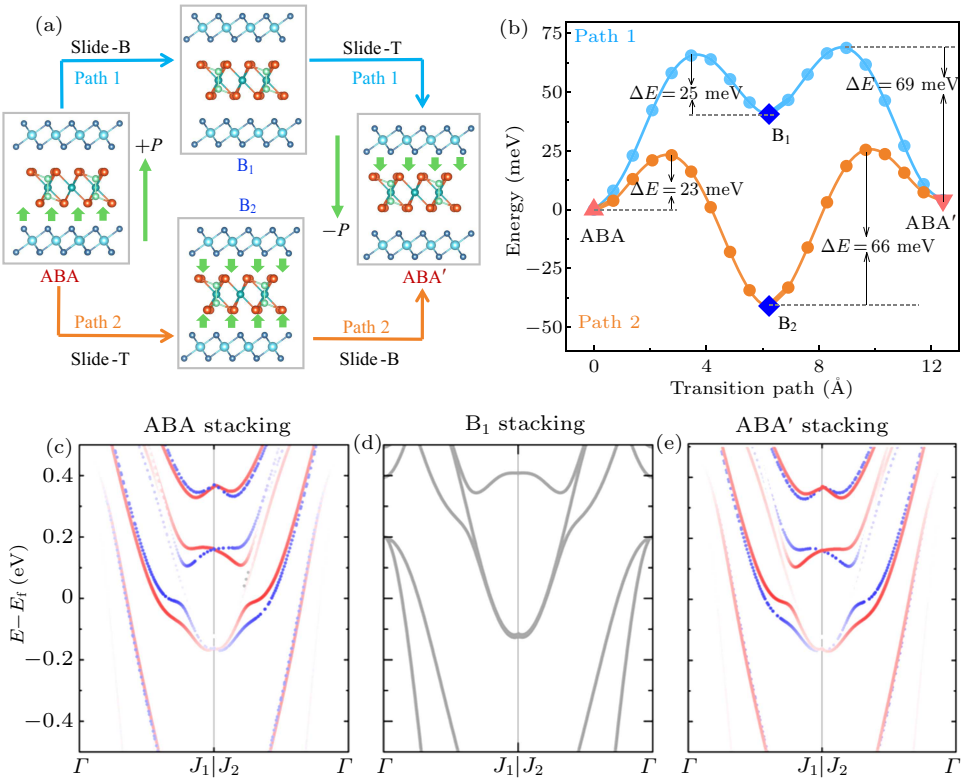


Fig. 4. Sliding-induced phase transition pathways and electronic structure evolution in the $SnS_2/CrSiTe_3/SnS_2$ sandwich heterostructure. (a) Schematic illustration of two nonequivalent sliding pathways and (b) the corresponding energy profiles. Path 1 (ABA → B_1 → ABA′) involves sequential sliding of the bottom layer (slide-B) followed by the top layer (slide-T), whereas path 2 (ABA→B_2→ABA′) proceeds in the opposite order. (c)–(e) Spin-resolved band structures (without spin–orbit coupling) of the ABA, B_1, and ABA′ stacking configurations along path 1, respectively. The high-symmetry points J_1 and J_2 denote the midpoints between K and M. Further details are provided in the supplemental material.[33] Solid (dashed) lines represent spin-up (spin-down) states. Red and blue colors indicate contributions from the two Cr magnetic sublattices corresponding to spin-up and spin-down orientations, respectively.

Band structure calculations confirm that pronounced nonrelativistic spin splitting emerges in both ABA and ABA′ configurations, with a maximum splitting of 59 meV near the Fermi level (Figs. 4(c) and 4(e)). This value represents an enhancement of approximately 40 meV compared to $MnPSe_3$-based systems.[18,27] During the sliding transition from ABA to ABA′, a 180° reversal of the polarization direction occurs simultaneously with the reversal of spin orientation, thereby forming a type-III multiferroic system characterized by deterministic spin-polarization locking. Interestingly, while the $CrSiTe_3/SnS_2$ bilayer heterostructure remains semiconducting, the $SnS_2/CrSiTe_3/SnS_2$ sandwich structure becomes metallic. This insulator-to-metal transition is primarily driven by the constructive superposition of interfacial dipoles, which gives rise to a substantially enhanced built-in electric field and induces a pronounced layer-dependent band realignment. The resulting field-driven band overlap leads to the emergence of metallicity in the heterostructure. A detailed analysis of this mechanism, including validation via layer-decoupling calculations (see Fig. S_2), is provided in Section 2 of the supplemental material.[33] In contrast, the B_1 and B_2 configurations, which preserve the D_{3d} point-group symmetry, exhibit fully spin-degenerate band structures; the band structure of the B_1 configuration is shown in Fig. 4(d).

Furthermore, when the interlayer distance is reduced from its equilibrium value of 3.3 Å to 3.0 Å and 2.8 Å, the enhanced interlayer coupling elevates the spin-splitting energy from 59 meV to 78 meV and 89 meV, respectively. This modulation is an order of magnitude larger than the effect achieved by an external electric field in $CrSiTe_3/SnS_2$ heterostructure ($E_z = 0.20$ V/Å), which induces a change of only ~ 2 meV. Such a significant enhancement underscores the superior efficacy of utilizing interlayer coupling — rather than external perturbation — to regulate the spin-splitting energy.

Compared to bilayer heterostructures, the fundamental advantage of the sandwich structure lies in the reversible regulation of its symmetry. Interlayer sliding enables flexible switching between the presence and absence of $\mathcal{P}$ symmetry, thereby inducing reversible phase transitions between AFM and AM states, and further realizing the switching and reversal of both electric polarization and spin polarization.

The preceding analyses of the $CrSiTe_3/SnS_2$ heterostructure and the $SnS_2/CrSiTe_3/SnS_2$ sandwich structure establish that the realization of spin-polarization locking type-III multiferroicity fundamentally originates from the dynamic control of $\mathcal{P}$ symmetry via interlayer sliding, rather than from specific chemical compositions. Although an external nonmagnetic substrate (e.g., SnS_2) facilitates symmetry breaking, it is not a prerequisite for achieving type-III multiferroicity.[18,40,41]

To verify the generality of this mechanism and eliminate lattice mismatch effects, a homostructural $CrSiTe_3/CrSiTe_3$ bilayer system is investigated. Similar to the heterostructures discussed above, two high-symmetry stacking configurations, namely AB [Fig. 2(a)] and BA, are considered for the $CrSiTe_3/CrSiTe_3$ bilayer. The AB stacking can be transformed into the BA stacking by applying an in-plane sliding of the bottom $CrSiTe_3$ layer by $\boldsymbol{r} = -1/3\boldsymbol{a}$.

Symmetry analysis shows that for both AB and BA stackings, the point-group symmetry is significantly reduced from D_{3d} (monolayer) to C_s, resulting in the complete removal of $\mathcal{P}$ symmetry. The band structures shown in Figs. 5(a) and 5(b) further confirm this behavior: both AB and BA configurations exhibit pronounced spin splitting, with the splitting at the conduction band edge reaching up to 59 meV, which is comparable to the values observed in the sandwich structure.

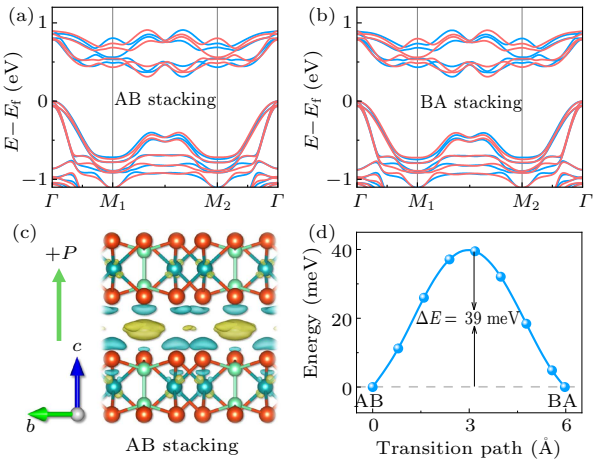


Fig. 5. Band structures and sliding-induced evolution of energy in the $CrSiTe_3/CrSiTe_3$ bilayer system. (a) and (b) Band structures of the AB and BA stacking configurations, respectively. (c) Charge density difference for the AB stacking configuration, with an isosurface value of 1.0×10^{-4} e/Å^3. (d) Energy evolution along the sliding pathway from AB to BA.

In the homostructure, the polarization arises from the relative displacement between interlayer Si–Te atomic pairs. The charge density difference ($\Delta\rho = \rho_{CrSiTe_3/CrSiTe_3} - \rho_{CrSiTe_3-up} - \rho_{CrSiTe_3-down}$) reveals that, for both AB and BA stacking configurations, the local environments of interfacial Te and Si atoms are inequivalent, leading to asymmetric charge redistribution along the out-of-plane direction [Fig. 5(c)]. At the upper interface, all Te atoms exhibit charge depletion. At the lower interface, Te atoms collinear with the Si–Si bonds along the z-direction show pronounced charge accumulation, while those collinear with Cr atoms exhibit charge depletion. This charge redistribution gives rise to an out-of-plane interfacial electric dipole oriented along the $+z$ direction. Therefore, the $CrSiTe_3$ bilayer also exhibits sliding ferroelectric behavior.

The band structure results of the $CrSiTe_3$ homostructure align perfectly with the symmetry analysis, exhibiting a simultaneous 180° reversal of both electric and spin polarizations during the AB to BA sliding transition. The calculated switching barrier for the sliding-induced switching process is 39 meV (~ 458 K) (Fig. 5(d)), which is higher than that reported for the $MnPSe_3/MnPSe_3$ bilayer system (31 meV).[18]

Nevertheless, the switching process can still be efficiently driven by relatively low external electric fields. In addition, the energy profile shows that the intermediate state corresponds to a local maximum, while both the initial and final states are located at potential-energy minima, ensuring robust nonvolatile stability of the ferroelectric and AM phases. These results demonstrate that reversible switching between AFM and AM states can be realized in bilayer $CrSiTe_3$ through interlayer sliding. This is consistent with earlier findings for $MnPSe_3$,[18,27] where the sliding process between AB and BA stackings is governed by the combined symmetry operation $\mathcal{P}\mathcal{C}_{2z}\mathcal{M}^{-1}$, which acts as an effective time-reversal operation when applied to the electronic bands. These findings establish that the engineering of type-III multiferroic states does not strictly necessitate an external substrate. Instead, a symmetry-compliant homostructural bilayer offers a versatile platform for realizing robust and switchable AM through purely intrinsic structural degrees of freedom.

3. Summary

We have demonstrated that $CrSiTe_3$-based van der Waals structures provide a versatile platform for realizing type-III multiferroicity, where AM is intrinsically coupled with sliding ferroelectricity. Interlayer sliding enables reversible control of $\mathcal{P}$ symmetry that connects the magnetic sublattices, thereby inducing transitions between conventional AFM and AM states. In the $CrSiTe_3/SnS_2$ heterostructure, breaking this sublattice-connecting $\mathcal{P}$ symmetry enables nonrelativistic spin splitting, but the absence of a $\mathcal{P}$ symmetry restoration pathway prevents full control of polarization and spin orientation. In contrast, the introduction of interlayer sliding degrees of freedom in the $SnS_2/CrSiTe_3/SnS_2$ sandwich structure enables switching between inversion-symmetric and inversion-broken states, which establishes a polarization-spin locking mechanism and allows for electrically controlled 180° reversal of spin polarization. Furthermore, investigations of the $CrSiTe_3/CrSiTe_3$ homostructure confirm the generality of this symmetry-driven mechanism. These findings reveal a general mechanism for coupling AM with sliding ferroelectricity and significantly broaden the application landscape of AM toward electrically controllable spintronic functionalities.

Acknowledgement

This work was financially supported by the National Natural Science Foundation of China (Grants Nos. 12474068, 12304103, and 12304104).

References

[1] Song C, Bai H, Zhou Z Y, Han L, Reichlova H, Dil J H, Liu J W, Chen X Z and Pan F 2025 *Nat. Rev. Mater.* **10** 473
[2] Smejkal L, Sinova J and Jungwirth T 2022 *Phys. Rev. X* **12** 040501
[3] Smejkal L, Gonzalez-Hernandez R, Jungwirth T and Sinova J 2020 *Sci. Adv.* **6** eaaz8809
[4] Šmejkal L, Sinova J and Jungwirth T 2022 *Phys. Rev. X* **12** 031042
[5] Liu H Z, He R, Zhan J Y, Wang D, He M D, Luo N N, Zeng J, Chen K Q and Tang L M 2025 *Phys. Rev. B* **112** 134411
[6] Huang F F, He S D, Chen K Q and Tang L M 2026 *Phys. Rev. B* **113** L020411
[7] Zhang F, Cheng X, Yin Z, *et al.* 2025 *Nat. Phys.* **21** 760
[8] Yan K, Cheng L, Hu Y, Gao J, Zou X and Chen X 2025 *Phys. Rev. Lett.* **134** 036302
[9] Li X, Zhu M, Dong J, Wu K, Zheng F and Zhang J 2025 *Chin. Phys. Lett.* **42** 100701
[10] He R, Wang D, Luo N N, Zeng J, Chen K Q and Tang L M 2023 *Phys. Rev. Lett.* **130** 046401
[11] Zhu H, Yu H, Zhu W, Yu G, Xu C and Xiang H 2025 *Phys. Rev. Lett.* **135** 196701
[12] Cheong S W and Mostovoy M 2007 *Nat. Mater.* **6** 13
[13] Ramesh R and Spaldin N A 2007 *Nat. Mater.* **6** 21
[14] Fiebig M, Lottermoser T, Meier D and Trassin M 2016 *Nat. Rev. Mater.* **1** 16046
[15] Wang J, Neaton J B, Zheng H, Nagarajan V, Ogale S B, Liu B, Viehland D, Vaithyanathan V, Schlom D G, Waghmare U V, Spaldin N A, Rabe K M, Wuttig M and Ramesh R 2003 *Science* **299** 1719
[16] Jiang J, Wu F, Wan Y, Li A, Huang C and Kan E 2025 *Phys. Rev. Lett.* **134** 196801
[17] Wang H, Liu H, Ye M and Li Y 2025 *Phys. Rev. Lett.* **135** 226402
[18] Sun W, Yang C, Wang W, Liu Y, Wang X, Huang S and Cheng Z 2025 *Adv. Mater.* **37** e2502575
[19] He R, Duan Z, Lei B, Luo N, Zeng J, Chen K Q and Tang L M 2025 *Phys. Rev. B* **112** 064423
[20] Zhang Y, Bai H, Zhang D, Chen C, Han L, Liang S, Chu R, Dai J, Sawicki M, Pan F and Song C 2025 *Chin. Phys. Lett.* **42** 027301
[21] Zhan J Y, He R, Wang D, He M D, Luo N N, Zeng J, Chen K Q and Tang L M 2025 *Phys. Rev. B* **112** 024408
[22] Li L and Wu M 2017 *ACS Nano* **11** 6382
[23] Yasuda K, Wang X, Watanabe K, Taniguchi T and Jarillo-Herrero P 2021 *Science* **372** 1458
[24] Vizner Stern M, Waschitz Y, Cao W, Nevo I, Watanabe K, Taniguchi T, Sela E, Urbakh M, Hod O and Ben Shalom M 2021 *Science* **372** 1462
[25] Wu M and Li J 2021 *Proc. Natl. Acad. Sci. USA* **118** e2115703118
[26] Bai Y, Yu Z, Guan Z, Tian J, Wang C, Yao X, Yang Y, Lei Y, Xu J, Liu C, Zhu J, Tu Y, Shen S, Xiang H, Li X, Xu C and Wang J 2025 *Nat. Commun.* **16** 7221
[27] Sun W, Wang W, Yang C, Hu R, Yan S, Huang S and Cheng Z 2024 *Nano Lett.* **24** 11179
[28] Dong P Q, Sun H B, Wu C and Li P 2026 *Acta Mater.* **309** 122064
[29] Bazazzadeh N, Hamdi M, Haddadi F, Khavasi A, Sadeghi A and Mohseni S M 2021 *Phys. Rev. B* **103** 014425
[30] Lin M W, Zhuang H L L, Yan J Q, Ward T Z, Puretzky A A, Rouleau C M, Gai Z, Liang L B, Meunier V, Sumpter B G, Ganesh P, Kent P R C, Geohegan D B, Mandrus D G and Xiao K 2016 *J. Mater. Chem. C* **4** 315
[31] Sivadas N, Daniels M W, Swendsen R H, Okamoto S and Xiao D 2015 *Phys. Rev. B* **91** 235425
[32] Chen X, Qi J and Shi D 2015 *Phys. Lett. A* **379** 60
[33] See supplemental material for computational details of the first-principles calculations, which includes Refs. [31,34-39].
[34] Kresse G and Hafner J 1993 *Phys. Rev. B* **47** 558
[35] Kresse G and Furthmuller J 1996 *Phys. Rev. B* **54** 11169
[36] Blöchl P E, Först C J and Schimpl J 2003 *Bull. Mater. Sci.* **26** 33
[37] Perdew J P, Burke K and Ernzerhof M 1996 *Phys. Rev. Lett.* **77** 3865
[38] Grimme S, Antony J, Ehrlich S and Krieg H 2010 *J. Chem. Phys.* **132** 154104
[39] Monkhorst H J and Pack J D 1976 *Phys. Rev. B* **13** 5188
[40] Sun W, Ye H, Liang L, Ding N, Dong S and Wang S S 2024 *Phys. Rev. B* **110** 224418
[41] Sun W, Yang C, Wang X, Huang S and Cheng Z 2026 *Nat. Mater.* **25** 884